The T Cell Receptor β Chain Repertoire of Tumor Infiltrating Lymphocytes Improves Neoantigen Prediction and Prioritization

Thi Mong Quynh Pham[1], Thanh Nhan Nguyen[1], Bui Que Tran Nguyen[1], Thi Phuong Diem Tran[1], Nguyen My Diem Pham[1], Hoang Thien Phuc Nguyen[1], Thi Kim Cuong Ho[1], Dinh Viet Linh Nguyen[1], Huu Thinh Nguyen[2], Duc Huy Tran[2], Thanh Sang Tran[2], Truong-Vinh Ngoc Pham[2], Minh-Triet Le[2], Thi Tuong Vy Nguyen[1], Minh-Duy Phan[1], Hoa Giang[1], Hoai-Nghia Nguyen[1], Le Son Tran[1]

1. Medical Genetics Institute, Ho Chi Minh City, Vietnam
2. University Medical Center Ho Chi Minh City, Ho Chi Minh City, Vietnam

* Correspondence:

Le Son Tran (leson1808@gmail.com), Hoai-Nghia Nguyen (nhnghia81@gmail.com)

Keywords: neoantigen, colorectal cancer (CRC), TCR sequencing (TCRseq), tumor variant calling, neoantigen identification workflow, neoantigen prioritization, cancer immunotherapy.

ABSTRACT

In the realm of cancer immunotherapy, the meticulous selection of neoantigens plays a fundamental role in enhancing personalized treatments. Traditionally, this selection process has heavily relied on predicting the binding of peptides to human leukocyte antigens (pHLA). Nevertheless, this approach often overlooks the dynamic interaction between tumor cells and the immune system. In response to this limitation, we have developed an innovative prediction algorithm rooted in machine learning, integrating T cell receptor β chain (TCRβ) profiling data from colorectal cancer (CRC) patients for a more precise neoantigen prioritization. TCRβ sequencing was conducted to profile the TCR repertoire of tumor-infiltrating lymphocytes (TILs) from 27 CRC patients. The data unveiled both intra-tumor and inter-patient heterogeneity in the TCRβ repertoires of CRC patients, likely resulting from the stochastic utilization of V and J segments in response to neoantigens. Our novel combined model integrates pHLA binding information with pHLA-TCR binding to prioritize neoantigens, resulting in heightened specificity and sensitivity compared to models using individual features alone. The efficacy of

our proposed model was corroborated through ELISpot assays on long peptides, performed on four CRC patients. These assays demonstrated that neoantigen candidates prioritized by our combined model outperformed predictions made by the established tool NetMHCpan. This comprehensive assessment underscores the significance of integrating pHLA binding with pHLA-TCR binding analysis for more effective immunotherapeutic strategies.

INTRODUCTION

In metastatic CRC patients, immunotherapy has fulfilled promise in improving survival rate (1). Immune checkpoint inhibitors (ICIs), which block negative regulatory pathways in T-cell activation, have been approved by the US Food and Drug Administration (FDA) for the treatment of deficient mismatch repair (dMMR) or high microsatellite instability (MSI-H) CRC patients (2-4). However, there is an urgent need for alternative immunotherapy strategies for metastatic CRC patients, as patients with proficient mismatch repair (pMMR) or microsatellite stability (MSS) have not shown significant responses to immune checkpoint inhibitors (2, 5).

Neoantigens (neopeptides) have emerged as potential targets for personalized cancer immunotherapy, including CRC (6, 7). Neoantigens are peptides that result from somatic mutations and can be displayed by class I human leukocyte antigen (HLA-I) molecules on the surface of cancer cells, thereby activating immune-mediated tumor killing (8). Recent studies have demonstrated that the presence of neoantigens is associated with better responses to immune checkpoint inhibitor (ICI) therapy in CRC patients (9, 10). A high neoantigen burden has been linked to improved overall survival and progression-free survival in patients with various solid tumors, including CRC (9, 10). Therefore, neoantigen-based immunotherapies are considered to have significant potential for improving treatment outcomes for CRC patients.

The successful development of neoantigen-based therapies hinges upon the identification of neoantigens that exhibit a strong binding affinity to their respective HLA-I molecules and demonstrate high immunogenicity. Initially, DNA sequencing of tumor tissues and paired white blood cells identifies cancer-associated genomic mutations, while RNA sequencing determines the patient's HLA-I allele profile and gene expression levels of mutated genes. *In silico* tools are then applied to analyze the tumor somatic variant, HLA-I allele, and gene expression data, predicting the binding affinity of neoantigens to the patient’s HLA-I alleles and their potential to activate T cell responses (11-13). This standard workflow has been successful in identifying clinically relevant neoantigens in various malignancies (12, 14).

However, despite its achievements, the current approach's impact on patient outcomes remains limited due to the scarcity of effective immunogenic neoantigens identified for each patient. This limitation arises primarily from the fact that the selection of neoantigen candidates by these workflows relies solely on neoantigen-HLA-I binding affinity as the criteria for immunogenicity prediction (15). While HLA-I binding is indeed a crucial factor for neoantigen presentation, it does not fully account for T cell receptor (TCR) recognition and interaction. The recognition of the neoantigen-HLA complex through TCR is of paramount importance for T cell activation and eliciting an immune response (16, 17). Various factors, such as the specific TCR repertoire, TCR clonality, and the structural characteristics of the TCR-peptide-HLA complex, profoundly influence TCR recognition. Unfortunately, these critical aspects are not entirely captured by HLA-I binding prediction alone.

The TCR is a critical component of the adaptive immune system, responsible for recognizing specific antigens presented by antigen-presenting cells (APCs). This membrane-bound heterodimer protein complex is expressed on the surface of T cells and exists in two distinct forms: TCRα/TCRβ for αβ T cells and TCRγ/TCRδ for γδ T cells, both intricately associated with invariant CD3 chain molecules (18, 19). TCR diversity arises from the recombination of variable (V), diversity (D), and joining (J) genes at the TCRβ and TCRδ loci, along with VJ recombination at the TCRα and TCRγ loci (20), giving rise to a broad array of unique TCRs collectively known as the TCR repertoire. The complementarity-determining region 3 (CDR3), situated at the junction of V, D, and J gene segments (21), plays a pivotal role in antigen recognition, with the unique combination of CDR3 sequences contributing significantly to the specificity and diversity of the TCR repertoire. With advancements in technology, TCR sequencing has become a powerful technique used to characterize the diversity and composition of TCR repertoires. Valuable information directly obtained through TCR sequencing, including TCR clonotype diversity, V(D)J gene usage, repertoire size, clonal expansion, and repertoire changes, has provided invaluable insights into immune responses, antigen recognition, and the development of targeted immunotherapies.

Sequencing the T cell receptors (TCRs) of TILs or lymphocytes found in peripheral blood provides crucial insights into the T-cell repertoire and their responses against neoantigens associated with tumors (22-24). This information holds paramount importance in identifying TCRs that specifically target these neoantigens. Additionally, it proves to be invaluable in

assessing the immunogenic potential of predicted neoantigens. Unfortunately, the current bioinformatic workflows used in neoantigen selection and prioritization do not incorporate TCR sequencing data. Therefore, we speculate that integrating TCR sequencing data into the assessment of immunogenicity of predicted neoantigens holds promise for unveiling effective neoantigens which can induce immune response, consequently, advancing the development of personalized immunotherapies for cancer.

To achieve this goal, we first performed TCR sequencing on frozen samples collected from CRC patients to profile TCRβ repertoire of tumor filtrating T cells. We next exploited the peptide-HLA (pHLA) and pHLA-TCR binding affinity of peptides with known immunogenicity status from six public databases including 10X Genomics (25-28), McPAS (29), PRIME (30), VDJdb (31), IEDB (32) and TBAdb (33) to develop a predictive algorithm. Subsequently, we employed this algorithm to predict and rank neoantigens by using the TCRβ, HLA types and mutation profiles identified from patients' frozen tumor tissues. Finally, we experimentally verified the efficacy of our model by measuring the immunogenicity of the ranked peptides by an ELISpot assay.

MATERIALS AND METHODS

Tumor biopsy and peripheral blood collection

Twenty-seven patients diagnosed with CRC were enrolled in this study at the University Medical Center in Ho Chi Minh City between June 2022 and May 2023. CRC confirmation was based on abnormal colonoscopies and histopathological analysis. The stages of CRC were determined according to guidelines provided by the American Joint Committee on Cancer and the International Union for Cancer Control (the eighth version) (34, 35). Prior to participation, all patients provided written informed consent for tumor and whole blood sample collection. Relevant clinical data, including demographics, cancer stages, and pathology information, were extracted from the medical records of the University Medical Center. Detailed information regarding the clinical factors of the patients can be found in **Table S1**. This study was approved by the Ethics Committee of the University of Medicine and Pharmacy in Ho Chi Minh City, Vietnam. For four patients, ten mL of peripheral blood was collected before surgery and stored in Heparin tubes prior isolation of PBMCs.

Targeted DNA, RNA and TCRβ sequencing

The DNA/RNA samples were isolated using either the AllPrep DNA/RNA Mini Kit or the AllPrep DNA/RNA/miRNA Universal Kit (Qiagen, Germany) as per the manufacturer's protocol. In addition, matched genomic DNA from the white blood cells (WBC) of individuals was also extracted from the buffy coat using the GeneJET Whole Blood Genomic DNA Purification Mini kit (ThermoFisher, MA, USA), following the manufacturer's instructions. Genomic DNA samples from the patients's paired tumor tissues and WBCs were used to prepare DNA libraries for DNA sequencing with the ThruPLEX Tag-seq Kit (Takara Bio, USA). The libraries were then pooled and hybridized with pre-designed probes for 95 targeted genes (Integrated DNA Technologies, USA). This gene panel encompasses commonly mutated genes in CRC tumors, as reported in the Catalog of Somatic Mutations in Cancer (COSMIC) database. The DNA libraries were then subjected to massive parallel sequencing on the DNBSEQ□G400 sequencer (MGI, Shenzhen, China) for paired-end reads of 2x100 bp with a sequencing depth of 10X .

Isolated total RNA was processed using the NEBNext Poly(A) mRNA Magnetic Isolation Module (New England Biolabs, MA, USA) to isolate intact poly(A)+ RNA following the manufacturer's instructions. RNA libraries were prepared using the NEBNext Ultra Directional RNA Library Prep Kit for Illumina (New England Biolabs). These libraries were subsequently sequenced for paired-end reads of 2x100 bp on an MGI system at a sequencing depth of 50X.

For TCRβ library construction, mRNA was utilized with the SMARTer Human TCR a/b Profiling Kit v2 (Takara, USA). The resulting libraries were sequenced for paired-end reads of 2x250 bp on an Illumina system at a sequencing depth of 7.5X.

Microsatellite instability status

Microsatellite instability (MSI) status was determined in both tumor DNA and corresponding DNA from blood, serving as the control, using the MSI Analysis System, version 1.2 (Promega, US). This analysis identified alterations in 5 mononucleotide repeat markers: BAT-25, BAT-26, NR-21, NR-24, and MONO-27. The results were classified as microsatellite stability (MSS) in cases where either none or only one marker was unstable. Samples showing alterations in two or more markers were categorized as microsatellite instability-high (MSI-H).

Variant calling from DNAseq and RNAseq data

The approach of integrating RNA-seq into calling variants was performed as described in our previous publication (36). Briefly, we used Dragen (Illumina) (37) in tumor-normal mode to detect somatic mutations from DNAseq data. The default filtering thresholds of Dragen were applied for the detection of single nucleotide polymorphisms (SNPs) and insertions/deletions (indels). SNPs were further filtered using the dbSNP and 1000 Genome datasets. Germline mutations in tumor tissues were identified by comparison with matched WBC DNA samples. Mutations within immunoglobulin and HLA genes were excluded due to alignment difficulties in these highly polymorphic regions, necessitating specialized analysis tools. Additionally, synonymous mutations were removed from downstream analysis. For analysis, we included somatic mutations that exceeded a minimum threshold of ≥2% variant allele frequency (VAF) in DNA extracted from fresh frozen tissues.

Sequencing reads underwent trimming using Trimmomatic (38) and were then aligned to the human reference genome using STAR (version 2.6.0c) (39). Prior to alignment, raw sequencing reads were subjected to quality checks using FastQC version 0.11.9 (40). VarScan 2 (41), , which accepts both DNA and RNAseq data, was employed to identify mutations in paired tumor and WBC samples across 95 cancer-associated genes. This analysis was carried out in tumor-normal mode. Four filtering steps were applied: (i) only calls with a PASS status were utilized, (ii) population SNPs overlapping with a panel of normal samples from the 1000 Genome dataset were excluded, (iii) somatic mutations included for analysis met a minimum threshold of ≥10× read depth and ≥2% variant allele frequency (VAF) in RNA extracted from FF tissue, and (iv) synonymous mutations and those related to HLA were removed from downstream analysis.

The resulting BAM files were sorted, indexed using Samtools version 1.10 (42), and had PCR duplicates removed using Picard tools version 2.25.6 (43). Somatic variants were manually reviewed using Integrative Genomics Viewer (v2.8.2). The VCF files generated by Dragen (for DNAseq) and VarScan 2 (for RNAseq) were subsequently annotated using the Ensembl Variant Effect Predictor (VEP version 105) (44) to extract information about the potential effects of variants on the phenotypic outcome.

CDR3β calling from TCRseq data

To define the CDR3β from TCRseq, we utilized Cogent NGS Immune Profiler Software v1.0 (45). Before calling clonotypes, the raw sequencing reads underwent filtering based on the following criteria: (i) allowing only one mismatch while splitting reads by matching read sequences to different receptor chains, (ii) excluding reads shorter than 30 bp and reads ambiguously matched to multiple receptor chains, (iii) excluding reads that failed correction when linker-based correction was enabled, (iv) excluding reads that failed the abundance check during sequencing error correction, and (v) excluding molecular identifier groups (MIGs) with fewer than 3 unique molecular identifier (UMI) reads. The filtered MIGs were then assembled and aligned to the V(D)J reference to define the TCR clonotype.

Shannon index and clonality

We utilized two indices to characterize T-cell diversity and expansion: the Shannon entropy index and the clonality index.

Shannon entropy:

$$-\sum_{i=1}^{n} p_i \log_e (p_i)$$

Clonality:

$$1 - \frac{\sum_{i=1}^{n} p_i \log_e(p_i)}{\log_e(n)}$$

These indices consider both the number of T-cell clone types 'n' and the frequency 'p_i' of each clone. Here, 'p_i' represents the proportion of the i-th clone within the TCR library containing n clones.

***In silico* prediction of peptide-HLA binding and peptide-HLA-TCR binding**

Class I HLA alleles (HLA-A/B/C) with two-digit resolution were identified from patient tumor RNAseq data using the OptiType tool (46). The annotated VCF files were analyzed using pVACseq, a tool in pVACtools (v1.5.9) (11, 47, 48). We used the default settings, except for disabling the coverage and MAF filters. We used all peptide-HLA-I binding algorithms that were implemented in pVACseq to predict 8 to 11-mer epitopes binding to HLA-I (A, B, or C) for downstream analysis. Mutants with lower binding affinity than wildtype peptides were

prioritized using a two-step ranking process. The minimum binding affinity score was calculated from the distribution of scores among the peptides derived from each mutation, and priority was given to mutations with the lowest binding affinity scores. Moreover, in pVACseq, we collected peptides with binding affinity scores lower than wildtype from multiple tools, calculated minimum binding affinity scores for each unique peptide, and incorporated this data into a combined machine learning model.

We used the peptide-HLA-TCR binding algorithm implemented in pMTNet (49) to predict peptide binding to HLA and TCR with default settings. These scores represented the predicted likelihood of peptides being immunogenic. A ranking value for immunogenicity was assigned to each unique peptide by determining the minimum TCR ranking of its immunogenicity score.

Construction of a combined machine learning model

To identify immunogenic peptides, we conducted a thorough search across multiple databases, including 10X Genomics (25-28), McPAS (29), VDJdb (31), IEDB (32), and TBAdb (33). For the creation of non-immunogenic peptides, we assembled a negative dataset using the PRIME tool (30). This dataset was generated by associating each peptide with 10 randomly generated TCRs sourced from the following databases: 10X Genomics, McPAS, VDJdb, IEDB, and TBAdb. To objectively evaluate the model, we separated the dataset mentioned above into two data subsets: discovery dataset (70%) and validation dataset (30%). peptides in the discovery dataset, whether labeled as immunogenic or non-immunogenic, were used for model training to classify whether a peptide is positive or not. Three machine learning algorithms, including Logistic regression (LR), Random Forest (RF), and Extreme Gradient Boosting (XGB), were examined for every feature type (pHLA binding, pHLA-TCR binding) and combined features. The 'CV' parameter (cross-validation) was set to 10. Selection of features was tested using a k-fold cross-validation approach on the training cohort with 'k' set to 10-fold, and the 'scoring' parameter was set to 'roc_auc'. The model cut-off was set based on a threshold specificity of >90% or >95% to achieve high specificity for selecting peptides. This combined model's performance was evaluated on the independent validation dataset of immunogenic and non-immunogenic peptides to assess its ability to classify positive peptides from negative peptides.

Ranking coverage score calculation

The approach of compare ranking between two algorithms was performed as described in a previous publication (50). Briefly, the rank coverage score was based on the ranking value calculation given by the formula:

$$\text{Rank Coverage Score} = \frac{\sum_{n \epsilon negative} \text{rank (n)}}{T \times \text{num (n)}} \times \text{coverage(n)} - \frac{\sum_{n \epsilon positive} \text{rank (p)}}{T \times \text{num (p)}} \times \text{coverage(p)}$$

$$\text{coverage (k)} = \frac{\text{max rank(k)}}{T} \quad k \epsilon (n, p)$$

Where, *T* presented the total neoepitope number identified and *p* and *n* presented the positive and negative peptides, respectively, that were experimentally validated in vitro.

If positive peptides have smaller rank values than negative peptides, this will result in a high rank coverage score, indicates the better ranking result.

Isolation, culture, and stimulation of PBMCs with long peptides

Peripheral blood samples were collected from four patients prior to surgery using BD Vacutainer Heparin Tubes (BD Biosciences, NJ, USA). Peripheral blood mononuclear cells (PBMCs) were isolated through gradient centrifugation using Lymphoprep (STEMCELL Technologies) within 4 hours of blood collection. The PBMCs were then resuspended in a solution of FBS (10%) and DMSO (7-10x10^6 cells/mL) for cryopreservation in liquid nitrogen. Frozen PBMCs were thawed in AIM-V media (Gibco, Thermo Scientific, MA, USA) supplemented with 10% FBS (Cytiva, USA) and DNase I (Stemcell Technology, Canada) (1 mg/mL) solution. A total of 10^5 PBMCs were allowed to rest in a 96-round bottom well-plate containing AIM V media supplemented with 10% FBS, 10 mM HEPES, and 50 mM β-mercaptoethanol overnight before stimulation with synthesized long peptides at a concentration of 5 mM in a humidified incubator at 37°C with 5% CO2. PBMCs were further stimulated with GM-CSF (2000 IU/mL, Gibco, MT, USA) and IL-4 (1000 IU/mL, Invitrogen, MA, USA) for 24 hours. Following this initial stimulation, LPS (100 ng/mL, SigmaAldrich, MA, USA) and IFN-γ (10 ng/mL, Gibco, MT, USA) were added to the PBMCs along with the peptides for an additional 12 hours. On the following day, IL-7, IL-15, and IL-21 (each at a concentration of 10 ng/mL) (Peprotech, NJ, USA) were added to the PBMC culture. The restimulation process involved exposing the peptides to fresh media containing IL-7, IL-15, and IL-21 every 3 days, for a total of 3 times. On day 12, PBMCs were restimulated with peptides and cultured in media without cytokines. ELISpot assays were performed on stimulated PBMCs on day 13.

ELISpot assay on PBMCs stimulated with long peptides

Cultured T cells were transferred to an enzyme-linked immunospot (ELISpot) plate (Mabtech, Sweden) and incubated for 20 hours at 37°C. Peripheral blood mononuclear cells (PBMCs) cultured with DMSO were used as a negative control group, while PBMCs stimulated with anti-CD3 were used as a positive control group. The ELISpot assay was performed on treated PBMCs using the ELISpot Pro: Human IFN-g (ALP) kit (Mabtech, Sweden), following the manufacturer's protocol. Developed spots on the ELISpot plate were then counted using an ELISpot reader (Mabtech, Sweden). Reactivity was determined by measuring the fold increase in the number of spots in PBMCs treated with mutant peptides compared to those treated with wild-type peptides. A fold change of two was selected as the cutoff for positivity, indicating a significant increase in reactivity.

Statistical analysis

In this study, t-tests were used to compare the TCR clones, clonality, and Shannon-index among two groups of four categories (Microsatellite status, stage, gender, tumor location). Chi-square test was used to compare the proportions of immununogenic and non-immunogenic peptides. All statistical analyses were performed using R (version 4.3.0) with common data analysis packages, including ggplot2 and pROC. The 95% confidence interval (95% CI) was presented in brackets next to a value as appropriate.

RESULTS

The workflow of identifying neoantigens by combining both HLA and TCR binding characteristics

The identification of neoantigens has traditionally heavily relied on peptide-HLA (pHLA) binding prediction while often neglecting the significance of pHLA-TCR interactions (49). In this study, we introduce a novel workflow that integrates both pHLA and pHLA-TCR interactions to enhance the precision of neoantigen identification and prioritization (**Figure 1**). In the first step (**Figure 1A**), we conducted RNA and DNA sequencing on matched tumor tissues and peripheral white blood cells (WBC) collected from 27 CRC patients to detect cancer-associated nonsynonymous mutations and determine HLA types, as detailed in our previous work (36). Additionally, T-cell receptor sequencing (TCR-Seq) was performed to profile the

TCRβ repertoire of TILs. In the second step (**Figure 1B**), we used the pVACseq and pMTNet tools to predict the binding affinities of both pHLA and pHLA-TCR interactions. To exploit the information of both pHLA and pHLA-TCR binding for selecting and ranking neoantigen candidates, we constructed a machine learning model by using immunogenic and non-immunogenic peptide information sourced from five publicly available databases (**Figure 1C**). Finally, we designed long peptide (LP) candidates encompassing the selected neoantigens and experimentally assessed their immunogenicity using peripheral blood mononuclear cells (PBMCs) obtained from the same patients (**Figure 1D**).

Heterogenous tumor infiltrating TCRβ profiles in colorectal cancer patients

Autologous TILs have exhibited varying reactivity levels to neoantigens, suggesting the potential of TIL-based recognition to improve the identification of immunogenic neoantigens (51). To explore this, we initiated our study by characterizing the TIL repertoire in a cohort of 27 colorectal cancer patients. This characterization involved sequencing the complementarity-determining region 3 (CDR3) of T-cell receptor beta (TCRβ), renowned for its remarkable diversity within the TCR gene. Our sequencing analysis yielded an average of 3,066,197 productive TCR reads per sample, with a range between 256,035 and 10,888,726 (**Supplementary Table 2**), following correction for duplications, sequencing errors, and exclusive use of uniquely barcoded reads mapped to TCRβ-CD3 sequences from the ImMunoGeneTics (IMGT) databases. Across the 27 patients, we observed variable numbers of TCRβ-CDR3 clonotypes, ranging from 433 to 27,749 (**Figure 2A & Supplementary Table 2,** 27 patients were arranged in ascending order), indicating the intra-tumor heterogeneity of TCR clonotypes. Of these clonotypes, 59.5% exhibited a single uniquely barcoded read mapped to the TCRβ-CDR3 sequences (depicted in yellow in **Figure 2A**), while 40.5% had at least two TCRβ-CDR3 reads confidently identified (**Figure 2A**). As observed previously (52), the length distribution of CDR3 was approximately normally distributed (median 14, range 4-43, **Supplementary Figure S1A**). Subsequently, we explored potential associations between TCR diversity, as quantified by the Shannon index, and patient characteristics. In accordance with prior investigations, we identified an inverse relationship between TCR clonality and the Shannon index (**Supplementary Figure S1**). However, we did not detect any significant correlations between TCR clonality or diversity and clinical variables, including microsatellite status, tumor staging, patient gender and tumor location (**Supplementary Figure S2**). In

contrast, MSI-H tumors, which are known to be rich in neoantigens (53, 54), displayed a significantly lower number of TCRβ clonotypes compared to MSS tumors (2185 versus 6070, p=0.047, **Supplementary Figure S2A**), aligning with previous research (55).

After filtering out TCR clones with read counts below 1, we obtained a total of 74,590 TCR clones. Subsequently, we conducted a comprehensive assessment of TCRβ repertoire similarity by calculating the proportion of overlapping TCRβ-CDR3 clones across the 27 patients. The preeminent majority, constituting 95.2% of all identified TCRβ-CDR3 clones, comprised unique clonotypes found in one patient, while the remaining 4.8% were recurrently observed in at least two patients (**Figure 2B**). This observation underscores the substantial inter-patient heterogeneity in TCR profiles. The TCRβ repertoire is generated by the random rearrangement of variable (V), diversity (D) and joining (J) segments. We conducted a search specifically targeting the D segment by scoring the similarities of sub-sequences within the junction sequences against the reference sequences of D segments. Consistent with a previous study, we were unable to unambiguously assign the D segments to any defined D region usage due to the truncation of this region (56). In contrast to the diversified D segments, V and J sequments displayed high recurrent rates across 27 patients (**Figure 2B**). As anticipated, we identified only 58 distinct V (**Figure 2C**) and 13 distinct J segments (**Figure 2D**), that collectively generated 184,396 clones across the 27 tumor tissue samples, underscoring the conservation of these segments (**Figure 2C & D**). Conversely, we observed a varied combination of V and J segments, which significantly contributes to the heterogeneity of the TIL TCRβ repertoire (**Figure 2E**). Collectively, our data elucidate the presence of both intra-tumor and inter-patient heterogeneity in the TCRβ repertoires of CRC patients, likely stemming from the stochastic utilization of V and J segments in response to neoantigens.

pHLA and pHLA-TCR interactions are two complement determinants of neoantigen immunogenicity

While *in silico* tools predicting HLA-peptide binding affinity have traditionally played a pivotal role in determining neoantigen immunogenicity (57), the evaluation of TCR-peptide binding for screening immunogenic neoantigens remains understudied. In light of this, our study aimed to assess the contributions of both pHLA and pHLA-TCR binding affinity in predicting immunogenic neoantigens. To accomplish this, we gathered HLA and TCRβ sequences from established datasets containing immunogenic and non-immunogenic peptides (**Supplementary**

Table 3). Subsequently, we employed NetMHCpan (13) and pMTNet (49) tools to predict pHLA and pHLA-TCR binding, respectively.

For comparative purposes, we generated plots depicting predicted percentile rank values, with lower percentile ranks signifying stronger binding affinity. As anticipated, our analysis revealed a significantly higher prevalence of peptides with robust HLA binding (percentile rank < 2%) among immunogenic peptides in contrast to their non-immunogenic counterparts (**Figure 3A & B**, $p < 0.00001$). Similarly, immunogenic peptides exhibited a greater proportion of peptides with percentile ranks indicating pHLA-TCR binding of < 2% compared to non-immunogenic peptides (**Figure 3C & D**, $p=0.086$). As recommended by NetMHCpan and pMTNet, we considered peptide candidates with predicted percentile ranks below 2% as binders. Utilizing this predefined threshold, both pHLA and pHLA-TCR binding affinity exhibited comparable positive predictive values (PPV), at 68.5% (**Figure 3B)** and 64.3% (**Figure 3D)**, respectively. This substantiates the significance of both pHLA and pHLA-TCR binding in determining the immunogenicity of peptides. When we simultaneously applied the cutoff values for both HLA-peptide and TCR-peptide percentile ranks (Q1 group, **Figure 3E**), the PPV increased to 76.9% from 68.5% and 64.3% for individual binding features (**Figure 3F**). This underscores the rationale for combining these two criteria to enhance the accuracy of neoantigen prediction. Notably, pHLA-TCR binding displayed a remarkedly lower sensitivity but higher specificity in comparison to pHLA binding (**Figure 3G**), implying their potential as a complementary criteria for the selection of immunogenic peptides.

Combination of peptide-HLA and peptide-HLA-TCR interactions improves neoantigen prediction

The combination of peptide-HLA and peptide-HLA-TCR binding ranking with a fixed cutoff values of 2% for each feature resulted in high specificity but low sensitivity (**Figure 3G**). To optimize the precision of immugenic neoantigens, we examined three distinct machine learning classifiers, namely Random Forest (RF), Logistic Regression (LR), and Extreme Gradient Boosting (XGB) classifiers. We first partitioned the pHLA binding and pHLA-TCR binding ranks for immunogenic and non-immunogenic peptides from publicly available databases into separate discovery and validation datasets. These datasets were used to develop and validate machine learning algorithms, as illustrated in **Figure 4A**. We next assessed the performance of the three examined algorithms, employing a 10-fold cross-validation strategy. Among these

algorithms, XGB demonstrated the highest performance, achieving an area under the receiver operating characteristic curve (AUC) of 0.82 in the training dataset and 0.84 in the validation dataset (**Supplementary Figure S3**). Consequently, the model combining pHLA and pHLA-TCR binding, referred to as the 'combined model' was chosen for further validation.

Our findings revealed that the combined model outperformed methods relying on pHLA-TCR or pHLA binding feature separately. The combined model yielded sensitivity AUC values of 0.82 (95% CI 0.81-0.84) and 0.84 (95% CI 0.82-0.86) for discovery and validation cohorts, whereas the pHLA-TCR feature alone achieved AUC values of 0.69 (95% CI 0.66-0.71) and 0.74 (95% CI 0.71-0.77). Meanwhile, the pHLA feature resulted in AUC values of 0.76 (95% CI 0.75-0.78) and 0.74 (95% CI 0.72-0.77) (**Figure 4B**). In order to address the elevated false positive rates associated with current prediction tools for neoantigens, we set the specificity at high thresholds of >95% and >99%. We observed that the combined model achieved a greater sensitivity (39.7% versus 5.9% and 19.7% at > 95% specificity; 47.1% versus 3.5% and 18.8% at > 99% specificity, **Figure 4C**), Negative Predictive Value (NPV, 87.7% versus 82% and 84.2% at > 95% specificity; 88.9% versus 81.5% and 83.9% at > 99% specificity, **Figure 4D**), and Positive Predictive Value (PPV, 65.9% versus 22.2% and 47.1% at > 95% specificity; 62.3% versus 11.8% and 39.4% at > 99% specificity, **Figure 4E**) compared to the single feature methods.

The accurate prioritization of neoantigen candidates with high immunogenicity holds the potential to streamline the validation process, reducing both costs and time expenditures. Consequently, we proceeded to evaluate the combined model's capacity to prioritize neoantigens by computing the ranking coverage score, which considers the accuracy in ranking immunogenic peptides versus non-immunogenic peptides (50). In the validation phase, the combined model exhibited superior rank coverage scores in comparison to the individual feature-based methods. The combined model attained a ranking coverage score of 0.37, while the single-feature methods, pHLA-TCR and pHLA, yielded scores of -0.26 and 0.25, respectively (**Figure 4F**). These findings underscore the notion that the incorporation of pHLA and pHLA-TCR binding criteria can enhance the accuracy of prediction and prioritization of immunogenic neoantigens.

Experimental validation of the pHLA-TCR and pHLA combined approach in selecting neoantigen candidates in patients with CRC

To experimentally validate the efficacy of our combined approach, we conducted a comparative analysis of the percentage of confirmed immunogenic neoantigen candidates and the ranking coverage scores between the conventional NetMHCpan method, which relies solely on pHLA binding percentiles, and our combined approach (**Figure 5A**). Due to the limited availability of patient blood samples, we were only able to perform validation on four patients who possessed sufficient quantity of PBMCs. For each patient, we chose the top three neoantigen candidates predicted by each method. Among the neoantigen candidates, three were found to be common between the two methods, while nine neoantigen candidates were uniquely identified by either NetMHCpan or the combined model (**Figure 5B**), bringing the total number of candidates to 21. Subsequently, we synthesized 21 long peptides (LPs) covering these 21 selected neoantigen candidates, along with 21 LPs corresponding to the wild-type sequences. The LPs were utilized in an *ex vivo* ELISpot assay to measure the release of interferon-gamma (IFNγ) from the four patients' PBMCs. If the stimulation with a mutant LP resulted in a > 2-fold increase in IFNγ spots compared to its corresponding wildtype LP, the respective neoantigen candidate was classified as an immunogenic neoantigen.

Out of the 21 selected LPs, we confirmed the immunogenicity of two LPs (RNF213_W719S and MAP3K1_L1202F) identified by the NetMHCpan method and four LPs (NCOR2_R1963H, TRRAP_F1568S, KMT2C_K3848T and SMAD4_G230R) selected by the combined method (**Figure 5C & 5D**). Notably, all four patients exhibited at least one immunogenic peptide identified by the combined method, whereas none of the LPs in two patients, PT07 and PT25, chosen via the NetMHCpan method were validated as immunogenic (**Figure 5C & 5D**). To further assess the ranking accuracy of these two methods, we calculated the ranking coverage scores. In agreement with our *in silico* analyses, we observed higher rank coverage scores for the combined method in three out of the four patients, resulting in an overall score of 0.02 (**Figure 5E**). In contrast, the NetMHCpan method exhibited a lower rank coverage score of -0.79 (**Figure 5E**). These outcomes conclusively demonstrate the ability of the combined approach to enhance the prediction and ranking of immunogenic neoantigens in cancer patients.

DISCUSSION

The selection of neoantigens plays a pivotal role in enhancing the efficacy of personalized treatments in cancer immunotherapy. Historically, neoantigen selection has predominantly hinged upon the prediction of peptide-human leukocyte antigen (pHLA) binding. However, the limitations of this approach have become increasingly evident (58), as it often neglects the dynamic interplay between tumor cells and the immune system. The findings of our study shed new light on this critical aspect of neoantigen selection. Our research highlights the potential of integrating pHLA binding prediction with the assessment of pHLA-Tumor-Infiltrating Lymphocyte T Cell Receptor (TIL TCR) binding (**Figure 1**). By encompassing the interaction between neoantigens and the tumor microenvironment, we have demonstrated a substantial enhancement in the accuracy of neoantigen selection and prioritization. Our findings underscore the significance of comprehensive neoantigen assessment in harnessing the full potential of immunotherapeutic strategies in the fight against cancer.

Our investigation into the TIL TCRβ repertoire across 27 CRC patients has unveiled a complex tapestry of intra-tumor and inter-patient heterogeneity (**Figure 2A &B, Supplementary Figure S2**). One underlying cause of this diversity is the random rearrangement of variable (V) and joining (J) segments, which contributes to the distinct TCRβ sequences observed (**Figure 2C, D &E**). This remarkable diversity in the TCRβ profile, as elucidated in our study, presents a potential link to the heterogeneity of cancer mutations and neoantigens within CRC. The intricate relationship between the TCRβ repertoire and the genetic alterations within the tumor microenvironment underscores the need for a more comprehensive understanding of this dynamic interplay to develop more precise immunotherapeutic strategies (59). Furthermore, our research revealed a compelling observation regarding patients with MSI-H, who are known to exhibit high mutation and neoantigen burdens (60, 61). Intriguingly, MSI-H patients with strong immune reactivity to neoantigens was shown to display a significantly lower number of TCR clonotypes and reduced diversity, as characterized by the Shannon index, compared to CRC patients with Microsatellite Stable (MSS) (**Supplementary Figure S2A**). This stark contrast in TCRβ diversity hints at the potential enrichment of neoantigen-reactive TCR clonotypes in MSI-H patients. These findings provide valuable insights into the immune responses to different subtypes of CRC and may guide the development of more tailored immunotherapies for patients with differing mutational landscapes.

By utilizing proven immunogenic and non-immunogenic peptides from public databases, we have demonstrated that predicting the strength of pHLA-TCR binding can be a crucial criterion for selecting immunogenic candidates (**Figure 3**). For the prediction of pHLA-TCR binding, we employed the well-established tool pMTnet (49). This choice was driven by its proven efficacy, based on its consistently high performance across different validated datasets (49). Although it exhibited lower sensitivity and positive predictive value (PPV) when compared to pHLA binding alone, pHLA-TCR binding strength exhibited notably superior specificity (**Figure 3G**). This implies that incorporating pHLA-TCR binding strength as a selection criterion would result in a reduced false positive rate, a crucial factor in the context of neoantigen selection. What makes our study particularly compelling is the convergence of these observations. The integration of both criteria, specifically, pHLA binding and pHLA-TCR binding strength, emerged as a strategy that not only enhanced the PPV but also fortified the rationale for combining these two features in the neoantigen selection process.

The integration of both pHLA binding and pHLA-TCR binding strength features in our approach exhibited superior performance in neoantigen selection and prioritization when compared to the single-feature method (**Figure 4**). This observation aligns with the findings of previous studies, which consistently indicate that combining multiple criteria enhances the accuracy and efficacy of neoantigen identification (50, 62). Furthermore, our experimental validation confirmed the robustness of our approach by consistently demonstrating performance consistent with our analysis on publicly available data (**Figure 5**). When examining the percentile ranks of positive LPs predicted by netMHCpan from those predicted by our combined model, the results further underscored the strength of our approach (**Figure 5E**). This alignment between experimental validation and computational analysis enhances the reliability and applicability of our neoantigen selection method. Interestingly, the four identified neoantigen candidates with confirmed immunogenicity by the combined approach have not been previously reported in public neoantigen databases, indicating that they could serve as novel targets for neoantigen based therapies.

However, several limitations must be acknowledged. Firstly, the relatively small sample size employed for validation raises the potential for ranking score bias. Additionally, while both TCRα and TCRβ regions play essential roles in engaging peptide-bound HLA complexes, our study focused solely on TCRβ sequences to predict pHLA-TCR binding strength. Future

investigations should include TCRα sequences to provide a more comprehensive analysis. Although the PBMC and TILs were previously shown to be congruent in neoantigen reactivity (63), it is important to recognize that differences in the contribution of TIL and PBMC TCR repertoires in neoantigen selection may introduce variability in the selection and validation of neoantigen candidates, and future studies are warranted to address the consistency in neoantigen reactivity between these two sources of T cells.

In summary, our study delves into the diversity and variation within the TCRβ repertoire of TILs in the tumor tissues of colorectal cancer patients. Through our research, we have introduced a novel approach for the identification and prioritization of neoantigen candidates. This approach combines the assessment of peptide-human leukocyte antigen (pHLA) binding and peptide-human leukocyte antigen-T cell receptor (pHLA-TCR) binding. Our findings underscore the significance of considering pHLA-TCR binding interactions as part of the process for selecting neoantigen candidates. This is a crucial step in the development of personalized immunotherapy strategies. By combining these two factors, we can more accurately identify the neoantigens that hold promise for effective immunotherapy, ultimately improving the prospects for tailored and effective cancer treatment.

Author contributions

Pham Thi Mong Quynh, Nguyen Thanh Nhan, Nguyen Bui Que Tran, Nguyen Hoang Thien Phuc, Tran Thi Phuong Diem, Pham Nguyen My Diem, Ho Thi Kim Cuong, and Nguyen Dinh Viet Linh were engaged in formal analysis, data curation, and methodology development for the manuscript draft. Huu Thinh Nguyen provided conceptualization and patient consultation. Duc Huy Tran, Tran Thanh Sang, Truong-Vinh Ngoc Pham, and Minh-Triet Le were responsible for patient recruitment and tissue histological analysis. Nguyen Thi Tuong Vy contributed to formal analysis and data curation. Minh-Duy Phan supported in conceptualization and manuscript editing. Hoa Giang contributed to conceptualization and methodology. Hoai Nghia Nguyen provided supervision and conceptualization guidance. Le Son Tran contributed to conceptualization and manuscript writing.

Acknowledgments

The authors thank all participants who agreed to take part in this study. We thank Dr. Kien Nguyen for proofreading our manuscript.

Financial & competing interests' disclosure

This research was funded by a NexCalibur Therapeutic grant (NC01). The authors including Le Son Tran and Minh Duy Phan hold the equity in NexCalibur Therapeutic.

FIGURE LEGEND

Figure 1. A novel workflow based on machine learning that integrates TCRβ sequencing data for the identification and ranking of CRC neoantigens.

(A) Tumor biopsies and peripheral blood from CRC patients were subjected to targeted DNA-seq, RNA-seq, and TCR-seq. (B) The prediction of peptide-HLA binding and peptide-HLA-TCR binding by indicated tools using the DNA-seq, RNA-seq, and TCR-seq data was performed. (C) Machine learning models were subsequently constructed based on the analysis of the peptide-HLA binding and peptide-HLA-TCR binding features to distinguish immunogenic antigens from non-immunogenic peptides. The immunogenicity of predicted neoantigen candidates prioritized by the model was validated by ELISpot to evaluate the effectiveness of this approach.

Figure 2. Tumor-infiltrating TCRβ profiles in 27 colorectal cancer patients.

(A) A bar plot depicting the distribution of TCR clonotypes among 27 CRC patients, categorized into two groups: those with a unique read count and those with read counts greater than or equal to 2 for each TCR clonotype. (B) The pie chart displays the recurrence rates of TCR clones, V segments, and J segments when the read count of TCR clones exceeds 01. The graph illustrates the uniqueness of TCR clones and the shared presence of both V and J segments. (C) The heatmap depicts the Z-scored read counts of V segments or (D) J segments across 27 samples. Some V and J segments were found to be dominant in all samples. (E) The chord diagram illustrates the rearrangement of V and J segments, revealing random V and J combinations, with a few combinations exhibiting high frequencies.

Figure 3. Peptide-TCR and peptide-HLA interactions are two complementary determinants of neoantigen immunogenicity.

(A) The histogram displays the HLA percentile distribution of immunogenic antigens (red bar) and non-immunogenic peptides (grey bar). (B) The percentage of immunogenic antigens (red bar) and non-immunogenic peptides (grey bar) is compared between two groups based on HLA

percentile: <2% and >= 2% (Chi-square test, p< 0.00001). (C) The histogram displays the TCR ranking distribution of immunogenic antigens (red bar) and non-immunogenic peptides (grey bar). (D) The percentage of immunogenic antigens (red bar) and non-immunogenic peptides (grey bar) is compared between two groups based on TCR ranking: <2% and >= 2% (Chi-square test, p=0.086). (E) The scatter plot illustrates the relationship between the HLA percentile distribution and TCR ranking of immunogenic antigens (red bar) and non-immunogenic peptides (grey bar). (F) The percentage of immunogenic antigens (red bar) and non-immunogenic peptides (grey bar) is analyzed in four distinct groups based on cutoffs of HLA percentile and TCR ranking. (G) The bar plot illustrates the sensitivity and specificity of three neoantigen prioritization approaches: based on neoantigen-HLA binding affinity alone (yellow bar), neoantigen-TCR binding ranking alone (blue bar), and the combined method using both features (red bar).

Figure 4. The combined model demonstrates improved sensitivity and specificity for neoantigen prioritization.

(A) The workflow for constructing the model. (B) The ROC curves demonstrate the performance of both the combined model and individual models in both the discovery and validation cohorts. The bar graphs illustrate the sensitivity (C), negative predictive value (NPV) (D), and positive predictive value (PPV) (E) at specificity levels of at least 95% or 99% for both the combined and individual models in both the discovery and validation cohorts. (F) Ranking coverage scores for the specified models in either the discovery or validation cohorts.

Figure 5. Validation of neoantigens identified *in silico* from the novel workflow through ELISpot assays conducted on four CRC patients.

(A) A schematic diagram illustrates the procedural steps of neoantigen prioritization and the ELISpot assay. (B) The count of neoantigens identified from each pipeline. (C) The fold change in IFN-γ spots, relative to the wildtype peptides, is shown for 21 long peptides. Note: Only the mutants that result in a positive value in ELISpot are depicted, along with their corresponding amino acid changes and their associated rankings. (D) ELISpot assays on six long peptides resulting in at least a 2-fold change in IFN-γ spots. (E) The bar graphs display rank coverage scores of validated long peptides identified from the NetMHCpan tool (blue bar) or the combined method (red bar) for individual patients and all patients.

Supplementary Figure 1. Quality control metrics for Tumor-Infiltrating Lymphocyte (TIL) TCRβ analysis.

(A) Distribution of CDR3β lengths in total TCR clones. (B) The scatter plot illustrates the relationship between Shannon-index and clonality.

Supplementary Figure 2. Association between TIL TCRβ profiles and patients' characteristics.

The bar plot and dot plot compare TCR clones, Shannon-index, and clonality between MSI-H and MSS (A, B, C), stage II and III (D, E, F), female and male gender (G, H, I), and distal and proximal tumor locations (K, L, M).

Supplementary Figure 3. The performance of three machine learning models with three different algorithms is evaluated using receiver operating characteristic (ROC) curves.

The curves depict the performance of the combined model in the discovery cohort (A) and the validation cohort (B)

Supplementary Table 1. Clinical Characteristics of 27 CRC patients

Supplementary Table 2. Quality metrics of TCRβ sequencing

Supplementary Table 3. Percentage of unique and expanded TCR clones from 27 CRC patients

Supplementary Table 4. List of immunogenic antigen and non-immunogenic peptides from public databases

REFERENCES

1. K. Ganesh *et al.*, Immunotherapy in colorectal cancer: rationale, challenges and potential. *Nat Rev Gastroenterol Hepatol* **16**, 361-375 (2019).
2. J. C. Dudley, M. T. Lin, D. T. Le, J. R. Eshleman, Microsatellite Instability as a Biomarker for PD-1 Blockade. *Clin Cancer Res* **22**, 813-820 (2016).
3. D. T. Le *et al.*, PD-1 Blockade in Tumors with Mismatch-Repair Deficiency. *N Engl J Med* **372**, 2509-2520 (2015).
4. M. J. Overman *et al.*, Nivolumab in patients with metastatic DNA mismatch repair-deficient or microsatellite instability-high colorectal cancer (CheckMate 142): an open-label, multicentre, phase 2 study. *Lancet Oncol* **18**, 1182-1191 (2017).

5. D. T. Le *et al.*, Mismatch repair deficiency predicts response of solid tumors to PD-1 blockade. *Science* **357**, 409-413 (2017).
6. Y. Yu *et al.*, Neoantigen-reactive T cells exhibit effective anti-tumor activity against colorectal cancer. *Hum Vaccin Immunother* **18**, 1-11 (2022).
7. V. M. Kim *et al.*, Neoantigen-based EpiGVAX vaccine initiates antitumor immunity in colorectal cancer. *JCI Insight* **5** (2020).
8. E. Blass, P. A. Ott, Advances in the development of personalized neoantigen-based therapeutic cancer vaccines. *Nat Rev Clin Oncol* **18**, 215-229 (2021).
9. D. Miao *et al.*, Genomic correlates of response to immune checkpoint therapies in clear cell renal cell carcinoma. *Science* **359**, 801-806 (2018).
10. M. Yarchoan, A. Hopkins, E. M. Jaffee, Tumor Mutational Burden and Response Rate to PD-1 Inhibition. *N Engl J Med* **377**, 2500-2501 (2017).
11. J. Hundal *et al.*, pVACtools: A Computational Toolkit to Identify and Visualize Cancer Neoantigens. *Cancer Immunol Res* **8**, 409-420 (2020).
12. Z. S. Chheda *et al.*, Novel and shared neoantigen derived from histone 3 variant H3.3K27M mutation for glioma T cell therapy. *J Exp Med* **215**, 141-157 (2018).
13. B. Reynisson, B. Alvarez, S. Paul, B. Peters, M. Nielsen, NetMHCpan-4.1 and NetMHCIIpan-4.0: improved predictions of MHC antigen presentation by concurrent motif deconvolution and integration of MS MHC eluted ligand data. *Nucleic Acids Res* **48**, W449-W454 (2020).
14. T. N. Schumacher, R. D. Schreiber, Neoantigens in cancer immunotherapy. *Science* **348**, 69-74 (2015).
15. I. Chen, M. Y. Chen, S. P. Goedegebuure, W. E. Gillanders, Challenges targeting cancer neoantigens in 2021: a systematic literature review. *Expert Rev Vaccines* **20**, 827-837 (2021).
16. C. Szeto, C. A. Lobos, A. T. Nguyen, S. Gras, TCR Recognition of Peptide-MHC-I: Rule Makers and Breakers. *Int J Mol Sci* **22** (2020).
17. S. Guerder, R. A. Flavell, T-cell activation. Two for T. *Curr Biol* **5**, 866-868 (1995).
18. M. S. Kuhns, H. B. Badgandi, Piecing together the family portrait of TCR-CD3 complexes. *Immunol Rev* **250**, 120-143 (2012).
19. J. P. Rast *et al.*, alpha, beta, gamma, and delta T cell antigen receptor genes arose early in vertebrate phylogeny. *Immunity* **6**, 1-11 (1997).
20. E. Rosati *et al.*, Overview of methodologies for T-cell receptor repertoire analysis. *BMC Biotechnol* **17**, 61 (2017).
21. K. W. Wucherpfennig, E. Gagnon, M. J. Call, E. S. Huseby, M. E. Call, Structural biology of the T-cell receptor: insights into receptor assembly, ligand recognition, and initiation of signaling. *Cold Spring Harb Perspect Biol* **2**, a005140 (2010).
22. N. Porciello, O. Franzese, L. D'Ambrosio, B. Palermo, P. Nistico, T-cell repertoire diversity: friend or foe for protective antitumor response? *J Exp Clin Cancer Res* **41**, 356 (2022).
23. Y. C. Lu *et al.*, Direct identification of neoantigen-specific TCRs from tumor specimens by high-throughput single-cell sequencing. *J Immunother Cancer* **9** (2021).
24. L. Mazzotti *et al.*, T-Cell Receptor Repertoire Sequencing and Its Applications: Focus on Infectious Diseases and Cancer. *Int J Mol Sci* **23** (2022).
25. https://www.10xgenomics.com/resources/datasets/cd-8-plus-t-cells-of-healthy-donor-1-1-standard-3-0-2.

26. https://www.10xgenomics.com/resources/datasets/cd-8-plus-t-cells-of-healthy-donor-2-1-standard-3-0-2.
27. https://www.10xgenomics.com/resources/datasets/cd-8-plus-t-cells-of-healthy-donor-3-1-standard-3-0-2.
28. https://www.10xgenomics.com/resources/datasets/cd-8-plus-t-cells-of-healthy-donor-4-1-standard-3-0-2.
29. N. Tickotsky, T. Sagiv, J. Prilusky, E. Shifrut, N. Friedman, McPAS-TCR: a manually curated catalogue of pathology-associated T cell receptor sequences. *Bioinformatics* **33**, 2924-2929 (2017).
30. J. Schmidt *et al.*, Prediction of neo-epitope immunogenicity reveals TCR recognition determinants and provides insight into immunoediting. *Cell Rep Med* **2**, 100194 (2021).
31. M. Shugay *et al.*, VDJdb: a curated database of T-cell receptor sequences with known antigen specificity. *Nucleic Acids Res* **46**, D419-D427 (2018).
32. R. Vita *et al.*, The Immune Epitope Database (IEDB): 2018 update. *Nucleic Acids Res* **47**, D339-D343 (2019).
33. W. Zhang *et al.*, PIRD: Pan Immune Repertoire Database. *Bioinformatics* **36**, 897-903 (2020).
34. M. B. Amin *et al.*, The Eighth Edition AJCC Cancer Staging Manual: Continuing to build a bridge from a population-based to a more "personalized" approach to cancer staging. *CA Cancer J Clin* **67**, 93-99 (2017).
35. G. J. Tong *et al.*, Comparison of the eighth version of the American Joint Committee on Cancer manual to the seventh version for colorectal cancer: A retrospective review of our data. *World J Clin Oncol* **9**, 148-161 (2018).
36. B. Q. T. Nguyen *et al.*, Improvement in neoantigen prediction via integration of RNA sequencing data for variant calling. *Front Immunol* **14**, 1251603 (2023).
37. V. J. Severine Catreux, Lisa Murray, Rami Mehio, Gavin Parnaby, Cooper Roddey, Michael Ruehle, Wei-Ting Chen, Fan Zhang. https://www.illumina.com/science/genomics-research/articles/dragen-shines-again-precisionfda-truth-challenge-v2.html.
38. A. M. Bolger, M. Lohse, B. Usadel, Trimmomatic: a flexible trimmer for Illumina sequence data. *Bioinformatics* **30**, 2114-2120 (2014).
39. A. Dobin *et al.*, STAR: ultrafast universal RNA-seq aligner. *Bioinformatics* **29**, 15-21 (2013).
40. S. Andrews (2010) FastQC: a quality control tool for high throughput sequence data. (Babraham Bioinformatics, Babraham Institute, Cambridge, United Kingdom).
41. D. C. Koboldt *et al.*, VarScan 2: somatic mutation and copy number alteration discovery in cancer by exome sequencing. *Genome Res* **22**, 568-576 (2012).
42. H. Li *et al.*, The Sequence Alignment/Map format and SAMtools. *Bioinformatics* **25**, 2078-2079 (2009).
43. http://broadinstitute.github.io/picard.
44. W. McLaren *et al.*, The Ensembl Variant Effect Predictor. *Genome Biol* **17**, 122 (2016).
45. https://www.takarabio.com/learning-centers/next-generation-sequencing/bioinformatics-resources/cogent-ngs-immune-profiler.
46. A. Szolek *et al.*, OptiType: precision HLA typing from next-generation sequencing data. *Bioinformatics* **30**, 3310-3316 (2014).

47. J. Hundal *et al.*, pVAC-Seq: A genome-guided in silico approach to identifying tumor neoantigens. *Genome Med* **8**, 11 (2016).
48. J. Hundal *et al.*, Accounting for proximal variants improves neoantigen prediction. *Nat Genet* **51**, 175-179 (2019).
49. T. Lu *et al.*, Deep learning-based prediction of the T cell receptor-antigen binding specificity. *Nat Mach Intell* **3**, 864-875 (2021).
50. C. Zhou *et al.*, pTuneos: prioritizing tumor neoantigens from next-generation sequencing data. *Genome Med* **11**, 67 (2019).
51. F. Chen *et al.*, Neoantigen identification strategies enable personalized immunotherapy in refractory solid tumors. *J Clin Invest* **129**, 2056-2070 (2019).
52. S. Hey *et al.*, Analysis of CDR3 Sequences from T-Cell Receptor beta in Acute Respiratory Distress Syndrome. *Biomolecules* **13** (2023).
53. V. Roudko *et al.*, Shared Immunogenic Poly-Epitope Frameshift Mutations in Microsatellite Unstable Tumors. *Cell* **183**, 1634-1649 e1617 (2020).
54. S. Maleki Vareki, High and low mutational burden tumors versus immunologically hot and cold tumors and response to immune checkpoint inhibitors. *J Immunother Cancer* **6**, 157 (2018).
55. L. Laghi *et al.*, Prognostic and Predictive Cross-Roads of Microsatellite Instability and Immune Response to Colon Cancer. *Int J Mol Sci* **21** (2020).
56. M. B. Yassai, Y. N. Naumov, E. N. Naumova, J. Gorski, A clonotype nomenclature for T cell receptors. *Immunogenetics* **61**, 493-502 (2009).
57. A. Vitiello, M. Zanetti, Neoantigen prediction and the need for validation. *Nat Biotechnol* **35**, 815-817 (2017).
58. E. S. Borden, K. H. Buetow, M. A. Wilson, K. T. Hastings, Cancer Neoantigens: Challenges and Future Directions for Prediction, Prioritization, and Validation. *Front Oncol* **12**, 836821 (2022).
59. K. Joshi *et al.*, Spatial heterogeneity of the T cell receptor repertoire reflects the mutational landscape in lung cancer. *Nat Med* **25**, 1549-1559 (2019).
60. R. Motta *et al.*, Immunotherapy in microsatellite instability metastatic colorectal cancer: Current status and future perspectives. *J Clin Transl Res* **7**, 511-522 (2021).
61. N. Xie *et al.*, Neoantigens: promising targets for cancer therapy. *Signal Transduct Target Ther* **8**, 9 (2023).
62. M. Muller *et al.*, Machine learning methods and harmonized datasets improve immunogenic neoantigen prediction. *Immunity* 10.1016/j.immuni.2023.09.002 (2023).
63. P. Malekzadeh *et al.*, Antigen Experienced T Cells from Peripheral Blood Recognize p53 Neoantigens. *Clin Cancer Res* **26**, 1267-1276 (2020).

Figure 01

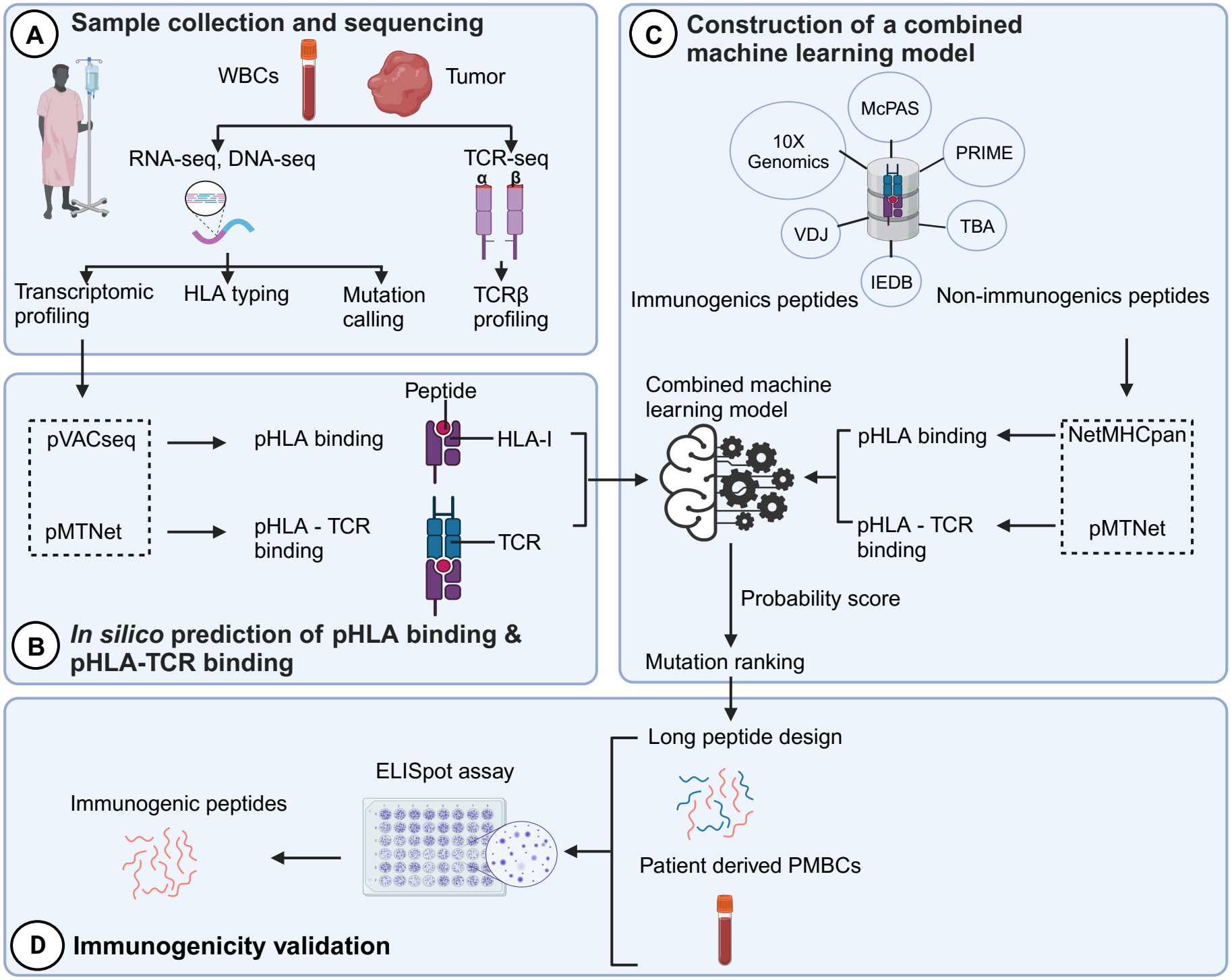
A
Sample collection and sequencing
WBCs
Tumor
RNA-seq, DNA-seq
TCR-seq
α
β
Transcriptomic profiling
HLA typing
Mutation calling
TCRβ profiling
B
In silico prediction of pHLA binding & pHLA-TCR binding
pVACseq
pMTNet
pHLA binding
pHLA - TCR binding
Peptide
HLA-I
TCR
C
Construction of a combined machine learning model
McPAS
10X Genomics
PRIME
VDJ
TBA
IEDB
Immunogenics peptides
Non-immunogenics peptides
Combined machine learning model
pHLA binding
pHLA - TCR binding
NetMHCpan
pMTNet
Probability score
Mutation ranking
D
Immunogenicity validation
Long peptide design
ELISpot assay
Immunogenic peptides
Patient derived PMBCs

Figure 02

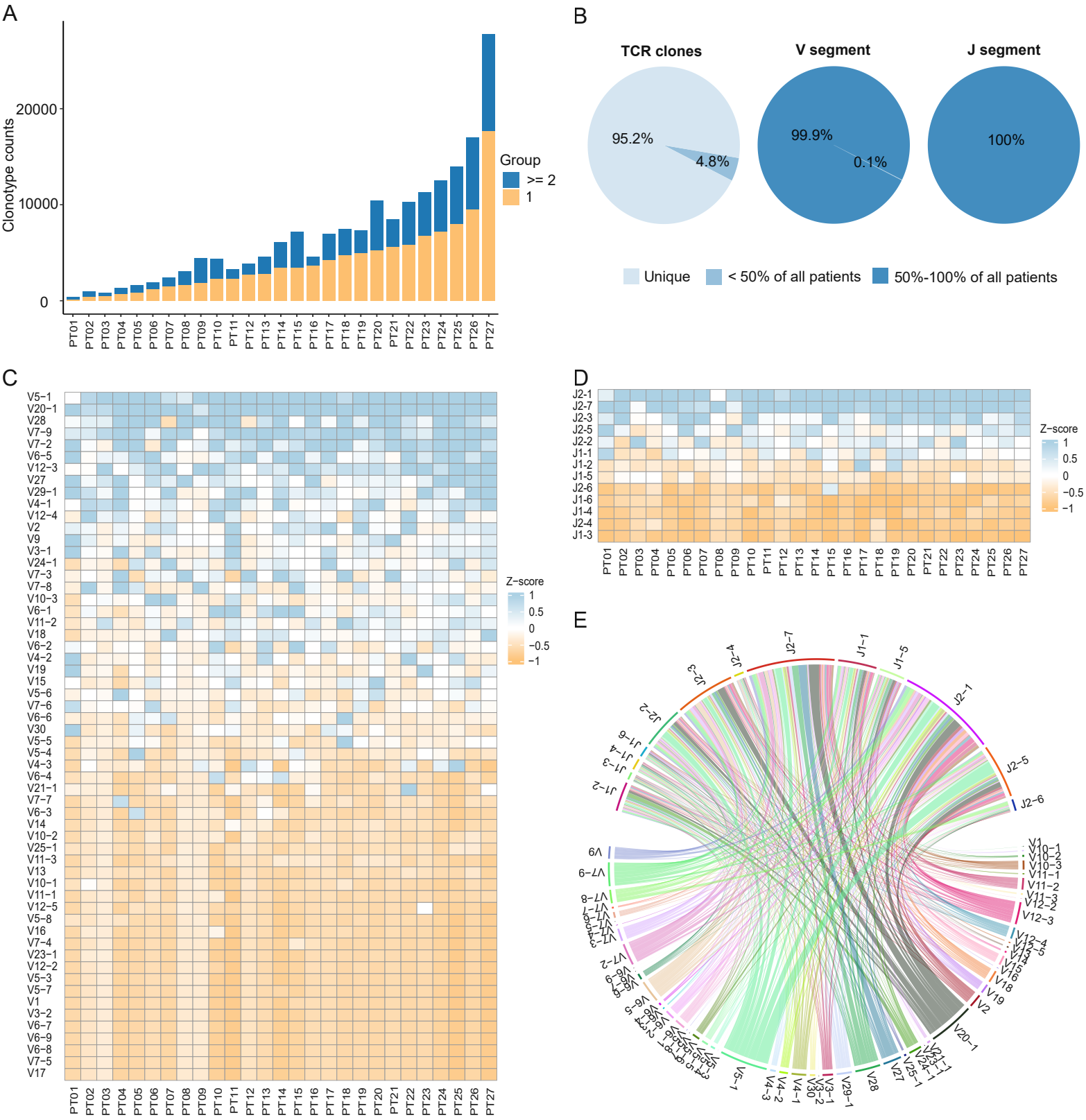
A
Clonotype counts
20000
10000
0
Group
>= 2
1
PT01 PT02 PT03 PT04 PT05 PT06 PT07 PT08 PT09 PT10 PT11 PT12 PT13 PT14 PT15 PT16 PT17 PT18 PT19 PT20 PT21 PT22 PT23 PT24 PT25 PT26 PT27
B
TCR clones
V segment
J segment
95.2%
4.8%
99.9%
0.1%
100%
Unique
< 50% of all patients
50%-100% of all patients
C
Z-score
1
0.5
0
−0.5
−1
D
Z-score
1
0.5
0
−0.5
−1
E

Figure 03

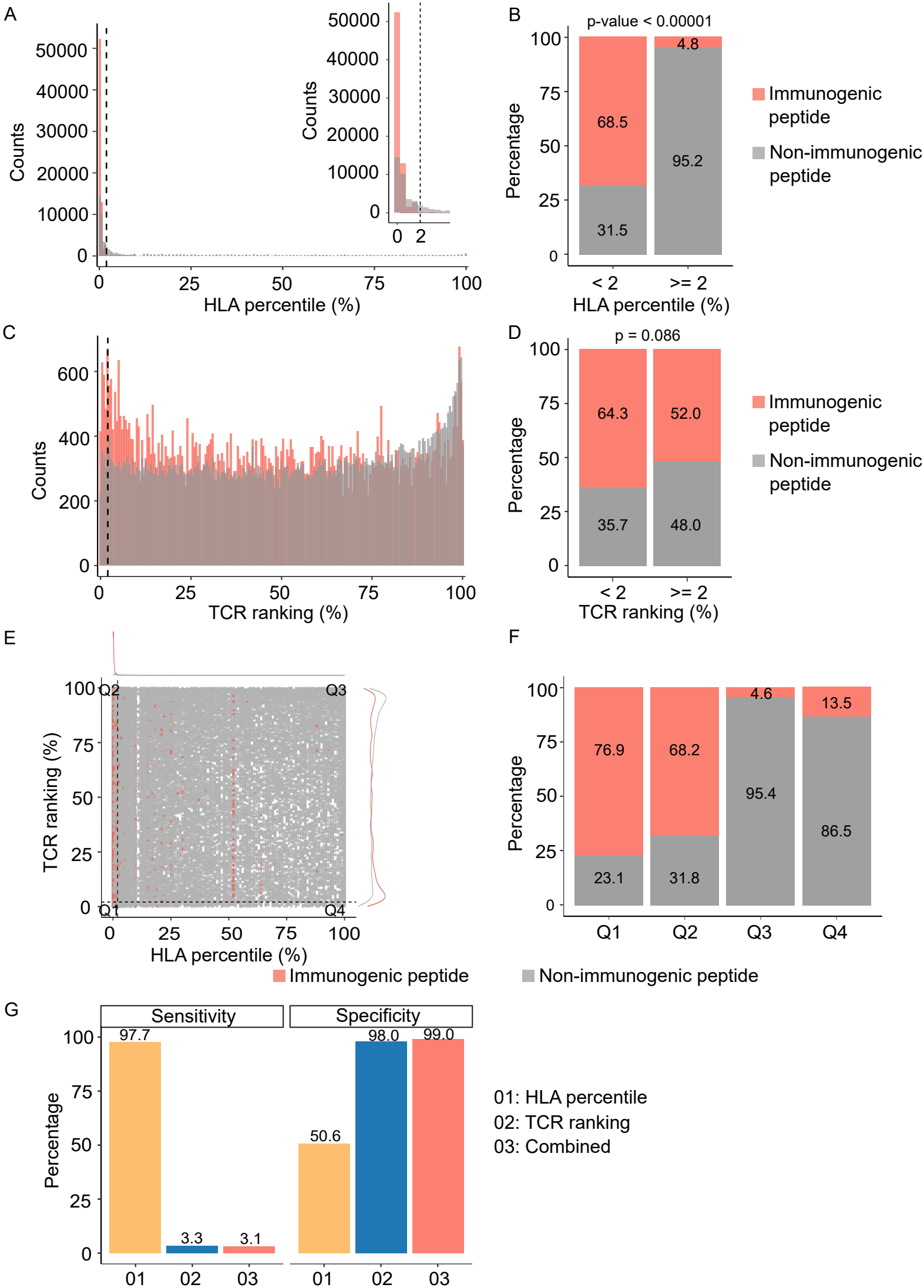
A
Counts
HLA percentile (%)
B
p-value < 0.00001
Percentage
68.5
31.5
4.8
95.2
< 2
>= 2
HLA percentile (%)
Immunogenic peptide
Non-immunogenic peptide
C
Counts
TCR ranking (%)
D
p = 0.086
Percentage
64.3
35.7
52.0
48.0
< 2
>= 2
TCR ranking (%)
Immunogenic peptide
Non-immunogenic peptide
E
Q1
Q2
Q3
Q4
TCR ranking (%)
HLA percentile (%)
F
Percentage
76.9
23.1
68.2
31.8
4.6
95.4
13.5
86.5
Q1
Q2
Q3
Q4
Immunogenic peptide
Non-immunogenic peptide
G
Sensitivity
Specificity
Percentage
97.7
3.3
3.1
50.6
98.0
99.0
01
02
03
01: HLA percentile
02: TCR ranking
03: Combined

Figure 04

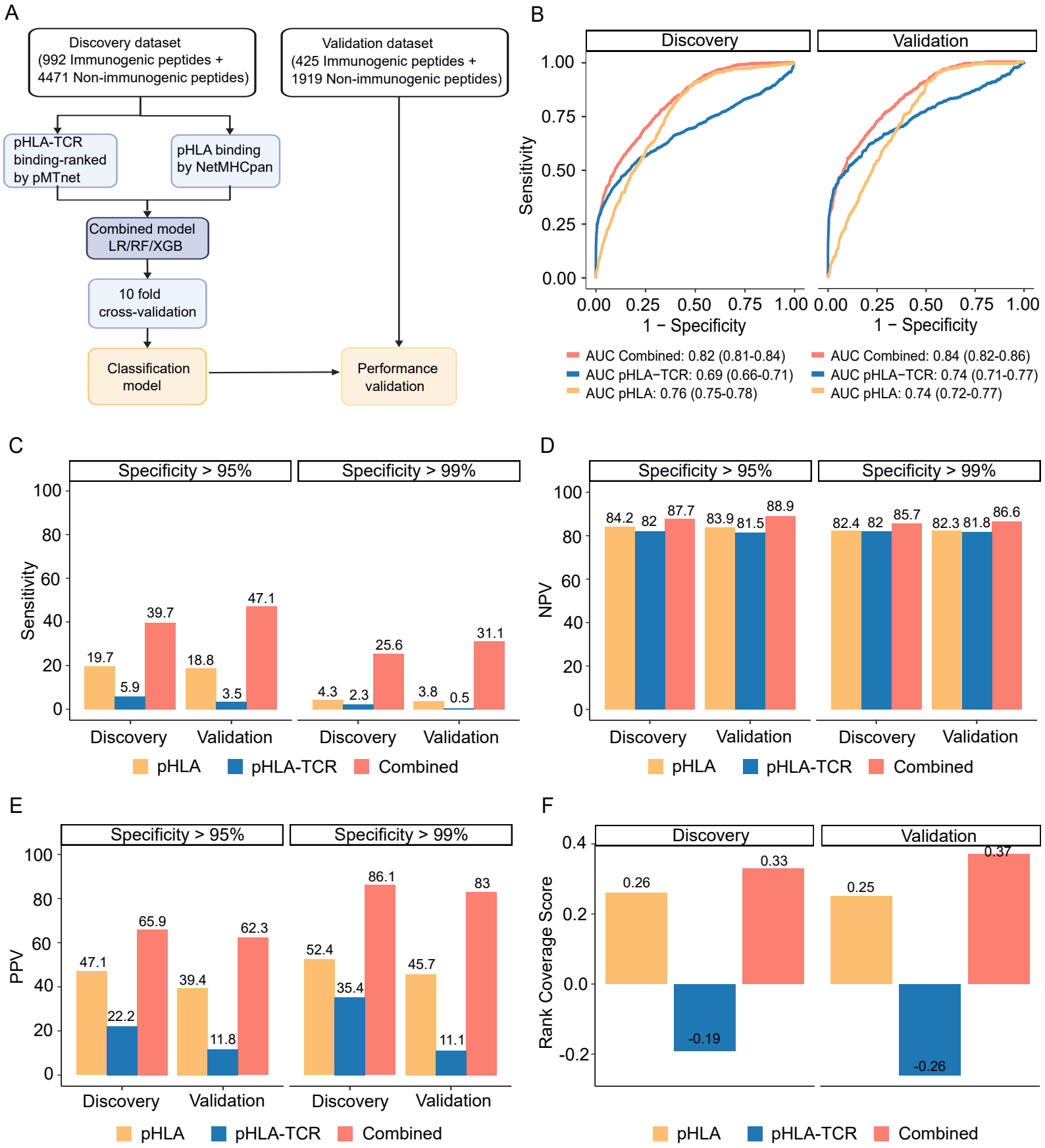
A
Discovery dataset
(992 Immunogenic peptides +
4471 Non-immunogenic peptides)
Validation dataset
(425 Immunogenic peptides +
1919 Non-immunogenic peptides)
pHLA-TCR
binding-ranked
by pMTnet
pHLA binding
by NetMHCpan
Combined model
LR/RF/XGB
10 fold
cross-validation
Classification
model
Performance
validation
B
Discovery
Validation
Sensitivity
1 − Specificity
AUC Combined: 0.82 (0.81-0.84)
AUC pHLA−TCR: 0.69 (0.66-0.71)
AUC pHLA: 0.76 (0.75-0.78)
AUC Combined: 0.84 (0.82-0.86)
AUC pHLA−TCR: 0.74 (0.71-0.77)
AUC pHLA: 0.74 (0.72-0.77)
C
Specificity > 95%
Specificity > 99%
Sensitivity
19.7
5.9
39.7
18.8
3.5
47.1
4.3
2.3
25.6
3.8
0.5
31.1
Discovery
Validation
pHLA
pHLA-TCR
Combined
D
NPV
84.2
82
87.7
83.9
81.5
88.9
82.4
82
85.7
82.3
81.8
86.6
E
PPV
47.1
22.2
65.9
39.4
11.8
62.3
52.4
35.4
86.1
45.7
11.1
83
F
Rank Coverage Score
0.26
-0.19
0.33
0.25
-0.26
0.37

Figure 05

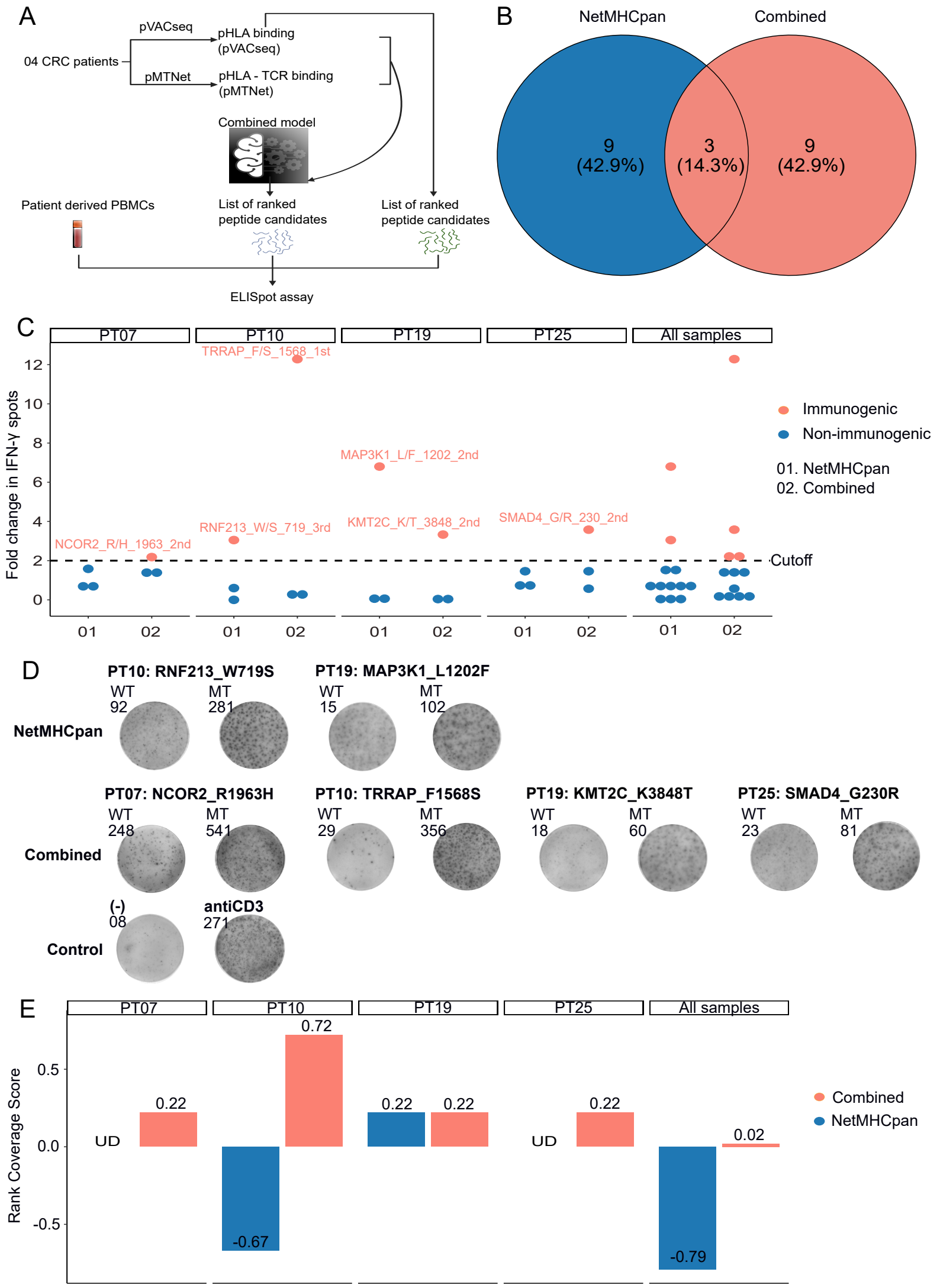
A
04 CRC patients
pVACseq
pMTNet
pHLA binding (pVACseq)
pHLA - TCR binding (pMTNet)
Combined model
Patient derived PBMCs
List of ranked peptide candidates
List of ranked peptide candidates
ELISpot assay
B
NetMHCpan
Combined
9 (42.9%)
3 (14.3%)
9 (42.9%)
C
PT07
PT10
PT19
PT25
All samples
Fold change in IFN-γ spots
TRRAP_F/S_1568_1st
MAP3K1_L/F_1202_2nd
NCOR2_R/H_1963_2nd
RNF213_W/S_719_3rd
KMT2C_K/T_3848_2nd
SMAD4_G/R_230_2nd
Cutoff
Immunogenic
Non-immunogenic
01. NetMHCpan
02. Combined
D
PT10: RNF213_W719S
WT 92
MT 281
PT19: MAP3K1_L1202F
WT 15
MT 102
NetMHCpan
PT07: NCOR2_R1963H
WT 248
MT 541
PT10: TRRAP_F1568S
WT 29
MT 356
PT19: KMT2C_K3848T
WT 18
MT 60
PT25: SMAD4_G230R
WT 23
MT 81
Combined
(-) 08
antiCD3 271
Control
E
PT07
PT10
PT19
PT25
All samples
Rank Coverage Score
UD
0.22
0.72
-0.67
0.22
0.22
UD
0.22
-0.79
0.02
Combined
NetMHCpan

Figure S01

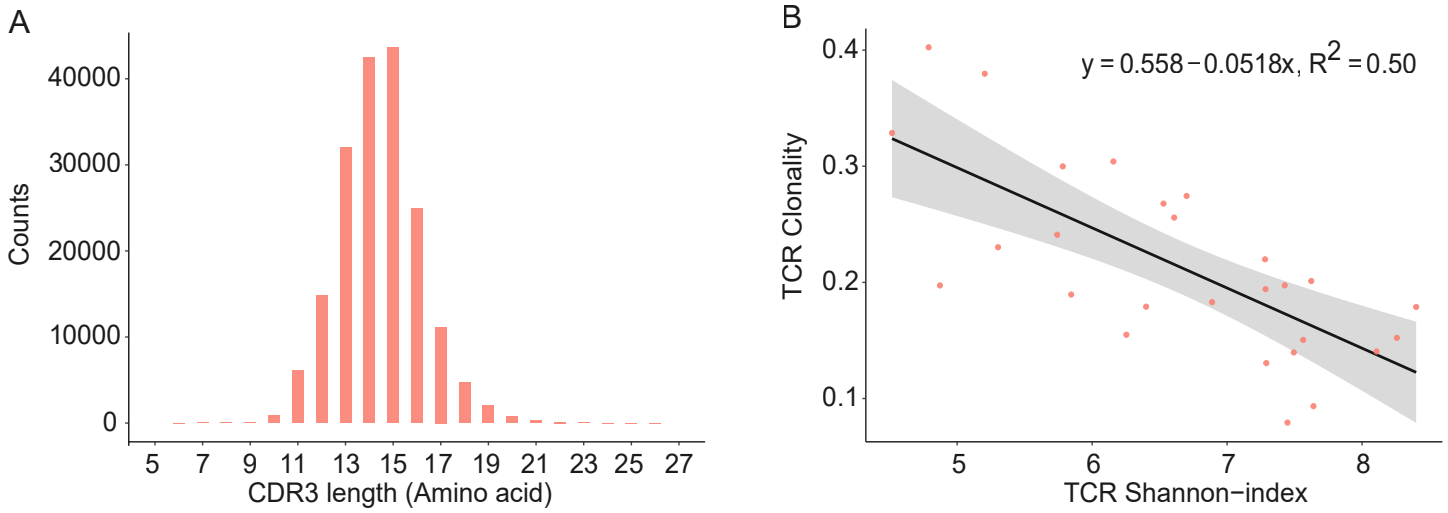
A
Counts
40000
30000
20000
10000
0
5 7 9 11 13 15 17 19 21 23 25 27
CDR3 length (Amino acid)
B
y = 0.558 − 0.0518x, R2 = 0.50
TCR Clonality
0.4
0.3
0.2
0.1
5 6 7 8
TCR Shannon−index

Figure S02

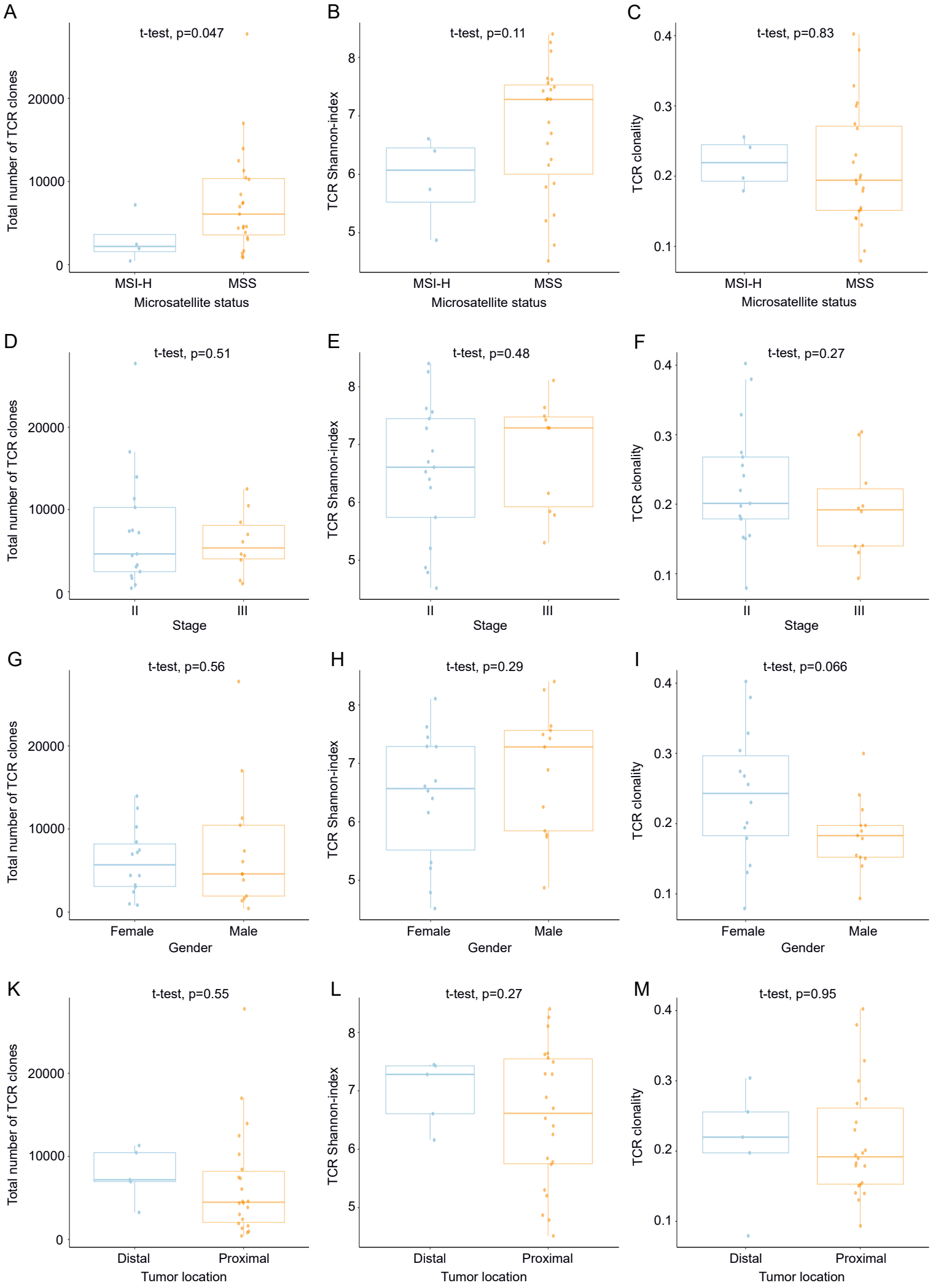
A
t-test, p=0.047
Total number of TCR clones
0
10000
20000
MSI-H
MSS
Microsatellite status
B
t-test, p=0.11
TCR Shannon-index
5
6
7
8
MSI-H
MSS
Microsatellite status
C
t-test, p=0.83
TCR clonality
0.1
0.2
0.3
0.4
MSI-H
MSS
Microsatellite status
D
t-test, p=0.51
Total number of TCR clones
0
10000
20000
II
III
Stage
E
t-test, p=0.48
TCR Shannon-index
5
6
7
8
II
III
Stage
F
t-test, p=0.27
TCR clonality
0.1
0.2
0.3
0.4
II
III
Stage
G
t-test, p=0.56
Total number of TCR clones
0
10000
20000
Female
Male
Gender
H
t-test, p=0.29
TCR Shannon-index
5
6
7
8
Female
Male
Gender
I
t-test, p=0.066
TCR clonality
0.1
0.2
0.3
0.4
Female
Male
Gender
K
t-test, p=0.55
Total number of TCR clones
0
10000
20000
Distal
Proximal
Tumor location
L
t-test, p=0.27
TCR Shannon-index
5
6
7
8
Distal
Proximal
Tumor location
M
t-test, p=0.95
TCR clonality
0.1
0.2
0.3
0.4
Distal
Proximal
Tumor location

Figure S03

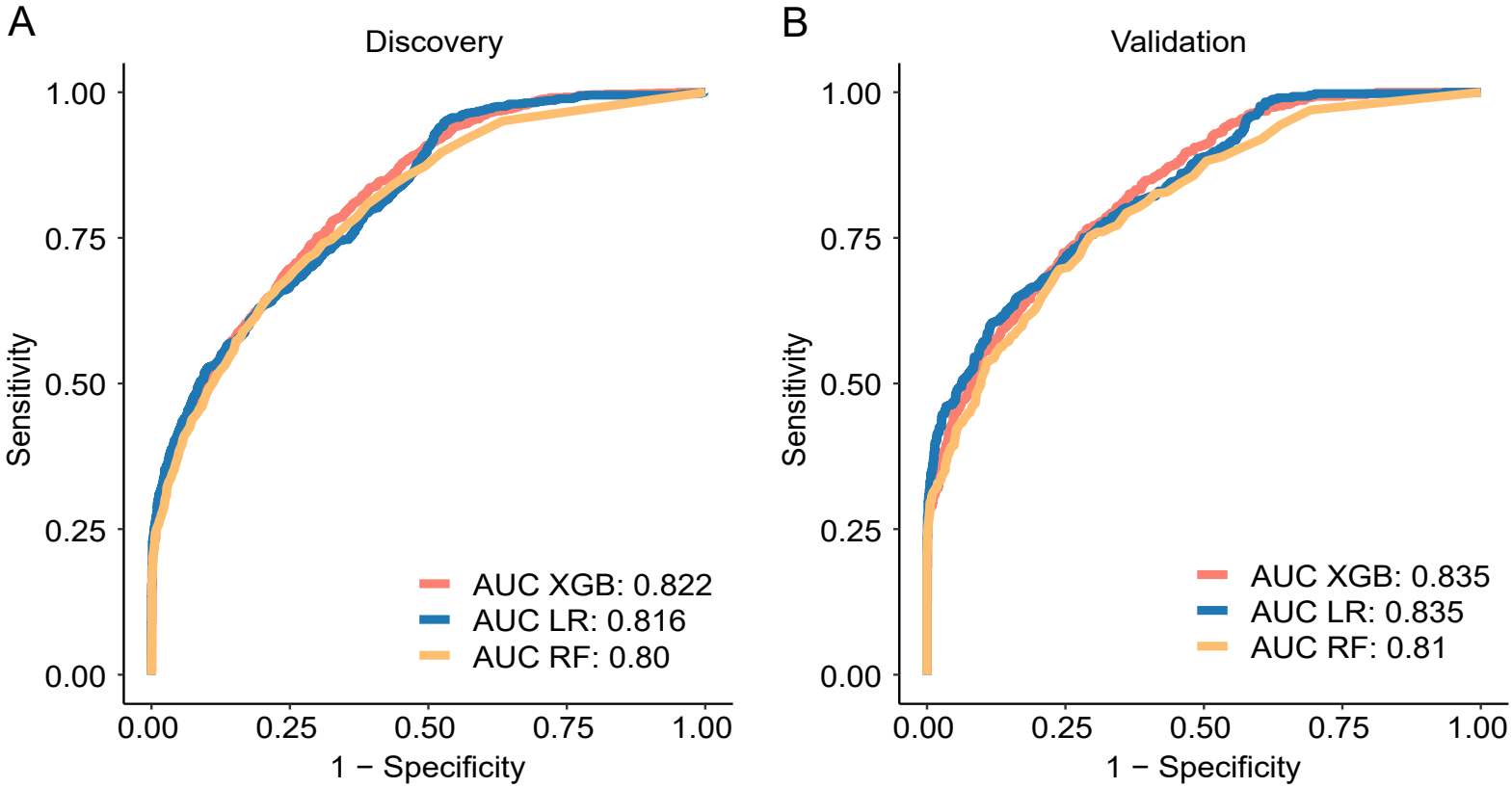
A
Discovery
Sensitivity
1 − Specificity
0.00
0.25
0.50
0.75
1.00
AUC XGB: 0.822
AUC LR: 0.816
AUC RF: 0.80
B
Validation
Sensitivity
1 − Specificity
0.00
0.25
0.50
0.75
1.00
AUC XGB: 0.835
AUC LR: 0.835
AUC RF: 0.81